Geant4 simulation of proton-induced single event upset in three-dimensional die-stacked SRAM device*

Bing Ye(叶兵)[1,†], Li-Hua Mo(莫莉华)[1,2], Tao Liu(刘涛)[3], Jie Luo(罗捷)[1], Dong-Qing Li(李东青)[1,2], Pei-Xiong Zhao(赵培雄)[1,2], Chang Cai(蔡畅)[1,2], Ze He(贺泽)[1,2], You-Mei Sun(孙友梅)[1], Ming-Dong Hou(侯明东)[1], and Jie Liu (刘杰)[1,‡]

[1] *Institute of Modern Physics, Chinese Academy of Sciences, Lanzhou* 730000, *China*
[2] *University of Chinese Academy of Sciences, Beijing* 100049, *China*
[3] *Science and Technology on Analog Integrated Circuit Laboratory, Chongqing* 400060, *China*

(Received 14 October 2019; revised manuscript received 3 December 2019; accepted manuscript online 9 December 2019)

Geant4 Monte Carlo simulation results of the single event upset (SEU) induced by protons with energy ranging from 0.3 MeV to 1 GeV are reported. The SEU cross section for planar and three-dimensional (3D) die-stacked SRAM are calculated. The results show that the SEU cross sections of the planar device and the 3D device are different from each other under low energy proton direct ionization mechanism, but almost the same for the high energy proton. Besides, the multi-bit upset (MBU) ratio and pattern are presented and analyzed. The results indicate that the MBU ratio of the 3D die-stacked device is higher than that of the planar device, and the MBU patterns are more complicated. Finally, the on-orbit upset rate for the 3D die-stacked device and the planar device are calculated by SPACE RADIATION software. The calculation results indicate that no matter what the orbital parameters and shielding conditions are, the on-orbit upset rate of planar device is higher than that of 3D die-stacked device.

Keywords: 3D-IC, single event upset, Geant4, proton

PACS: 61.82.Fk, 61.80.Jh, 42.88.+h **DOI:** 10.1088/1674-1056/ab5fc4

1. Introduction

Although the lithography equipment factory has confirmed the feasibility of technological development below 3 nm, it may not be simple if the IC industry relies solely on extreme ultraviolet lithography to maintain Moore's law. Thus, the chipmakers must now seek for the innovation in different directions in process and packaging technologies. For example, packaging technology is currently moving toward three-dimensional (3D) stacking. Compared with two-dimensional (2D) planar devices, 3D-IC no longer pursues the reduction of transistor size but increase the integration of the system through 3D stacking and realize the vertical interconnection between layers through through-silicon-via technology. Now, the 3D-IC has become one of the industry's recognized effective means of continuing Moore's law.[1] The advantages of high integration, small size and low power consumption of the 3D-IC make it have broad prospects and application value in the aerospace field.[2] For example, the 3D PLUS company's 3D-IC products are expanding continuously, and launched into space almost every month for deep space exploration missions and satellites constellation fleets.[3] It is also because of the broad application prospects of 3D-IC in the aerospace field, its irradiation effect has also received the researcher's attention.[4–11] Zhang *et al.* made the first significant attempt to characterize the microarchitecture soft error vulnerabilities across the stacked chip layers under 3D integration technologies.[4] They showcased that alpha particles induced by package material only affect the top layers of the 3D-IC because the outer layers have a shielding effect on inner layers. In 2011, Gouker *et al.* conducted a series of studies on single event upset (SEU) and single event transient for 3D-IC fabricated in Silicon-On-Insulator technology.[5,6] Since heavy ions have a higher linear energy transfer (LET) than proton, more energy can be deposited in the device, and more electron-hole pairs are generated, so most of the researches have focused on single event effect induced by heavy-ion. For example, Cao X *et al.* conducted a Geant4 simulation on heavy ions induced SEU for 3D integrated SRAM. Their simulated results show that the sensitivity of 3D SRAMs is not more than that of planar SRAMs and the 3D structure can have a great potential application for aerospace and military domain.[11]

In this paper, we construct a 3D die-stacked device model by using Geant4 simulation tool.[12] A detailed simulation study of the SEU of this 3D device caused by protons is carried out. The multi-bit upset (MBU) probability of the device is studied, and the MBU patterns are also analyzed in this paper. Finally, the on-orbit SEU rates of these two types of devices

*Project supported by the National Natural Science Foundation of China (Grant Nos. 11690041 and 11675233) and the Fund from the Science and Technology on Analog Integrated Circuit Laboratory, China (Grant No. JCKY2019210C054).

†Corresponding author. E-mail: yebing@impcas.ac.cn
‡Corresponding author. E-mail: j.liu@impcas.ac.cn

are also estimated and compared.

The rest of this paper is organized as follows. In Section 2, a detailed simulation setup is provided. In Section 3, the simulated result of proton-induced SEU in the 3D die-stacked device is presented. In Section 4 the SEU difference between the planar and 3D die-stacked device are discussed. Finally, some conclusions are drawn from the present study in Section 5.

2. Simulation setup

A single-layered SRAM model is constructed in Geant4 according to Ref. [13]. As shown in Fig. 1, this model including a single die with 25×25 cells in a cube with a size of 12.5 μm×31.25 μm×24 μm, the SEU critical charge of this device is set to be 0.8 fC. The primary proton energy set during the simulation is in a range of 0.3 MeV–100 MeV, and the energy deposited in the sensitive volume (SV) is recoded. The critical deposited energy is a minimum energy that causes the device to upset in the SV. When the deposited energy in SV exceeds the critical deposited energy, an SEU is recorded and the position information of the SV cell is given. By setting the initial energy of the incident proton, the variation of SEU cross-section of the device with proton energy is obtained and then compared with previous experimental data.

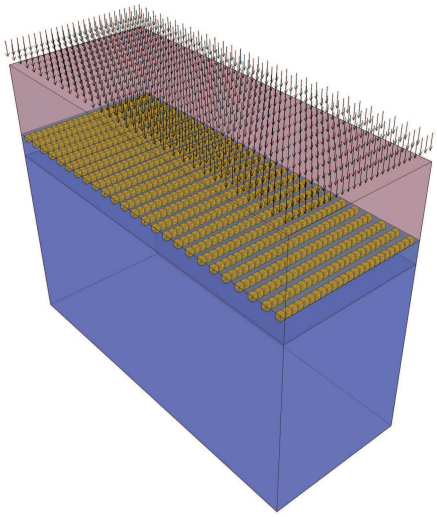

Fig. 1. Sketch of single-layered SRAM model.

As shown in Fig. 2, the SEU cross-section is given as a function of incident proton energy. Figure 2(a) shows Geant4 simulations on this single-layered SRAM model and figure 2(b) displays the precious experimental results of a 65-nm SRAM cited from Ref. [14]. As can be seen from Fig. 2, although the feature sizes of the two devices may be inconsistent with each other, the proton-induced SEU cross-section curve of the single-layered SRAM model and the previous 65-nm SRAM experimental results are still in good agreement. For example, the SEU cross-section caused by high-energy protons is about 4–5 orders of magnitude lower than the peak value of the SEU cross-section caused by low-energy protons (LEPs). The simulated SEU cross-section peak value caused by LEP is higher than the experimental result, which should be caused by the proton beam energy straggling as discussed in Ref. [15].

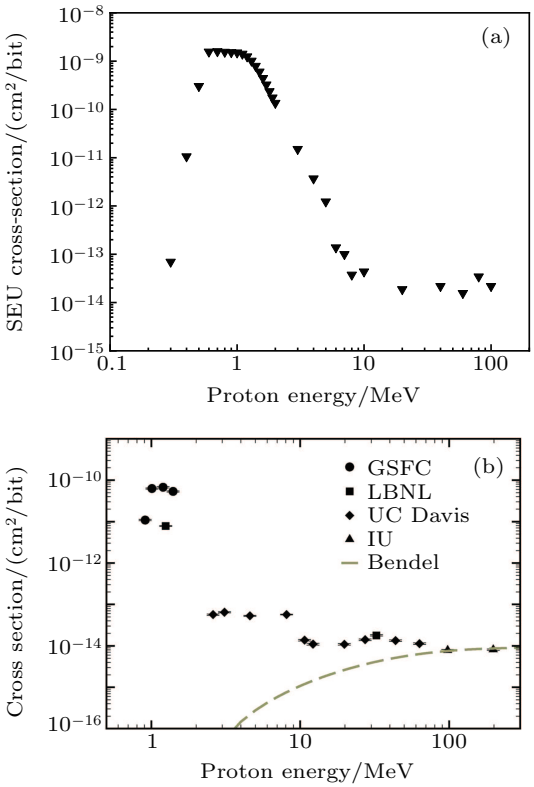

Fig. 2. Proton-induced SEU cross-section curves, showing (a) Geant4 simulations for single-layered SRAM model in this paper and (b) testing result for 65-nm SRAM in Ref. [14].

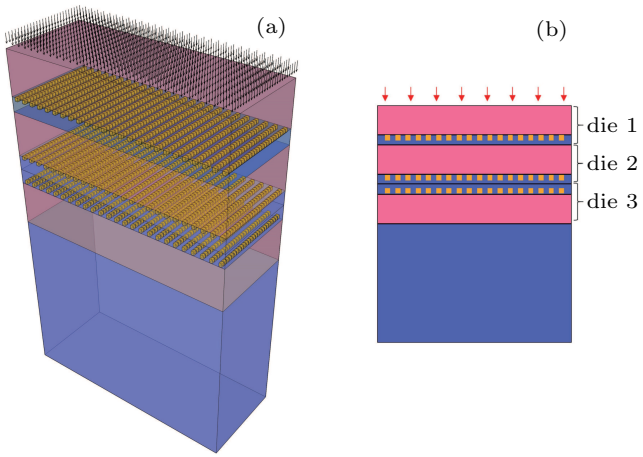

Fig. 3. Sketches of the three-layered die-stacked SRAM device model used in simulation: (a) 3D view and (b) Y–Z cross-section view (not scaled).

To further study the proton-induced SEU sensitivity of the 3D die-stacked device, we establish a three-layered stacked device model based on this single-layered SRAM model. As shown in Fig. 3, the simulation model is comprised of three dies in a cube with a size of 12.5 μm×31.25 μm×48 μm, and each die includes 25×25 SRAM cells. The first and the second layer die are bonded face-to-face structure, and the third

layer die is boned back-to-face structure with the second layer die. The size setting of the SV and the setting of the upset critical charge are the same as those of the single-layered SRAM model described above.

3. Simulation results

To improve the accuracy of the simulation, at least 100 upsets are recorded in each simulation. The SEU cross-section is calculated from

$$\sigma = N/(F \times 625 \times L),$$

where N is the number of recorded upsets in each simulation, F is the total fluence of proton in units protons/cm^2, and L is the number of die layers of the device. $L = 1$ refers to the single-layered die device and $L = 3$ the whole three-layered die-stacked device model. For each proton incident in this 3D die-stacked device, if the SEU sensitivity is uniform at each layer, then the final SEU cross-section of this whole model and the SEU cross-section of each layer are identical.

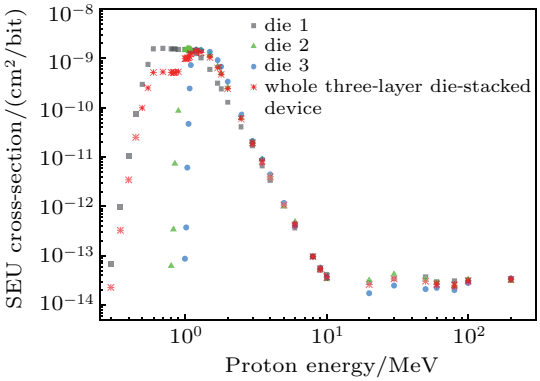

Fig. 4. Proton-induced SEU cross-section *versus* proton energy for three-layered die-stacked SRAM device model.

The Geant4 simulated SEU result of this three-layered die-stacked SRAM device model is shown in Fig. 4. As illustrated in this figure, the SEU cross-section of each layer and the entire device model are calculated, and the overall trend of the SEU cross-section of this three-layered die-stacked device is consistent with that of a single-layered die. The SEU cross-sections of their high-energy proton ranges are almost identical, and then an SEU cross-section peak appears in the LEP range, and this cross-section peak is about five orders of magnitude higher than the high-energy proton region. However, there are also some differences in specific detail, especially in area where the proton energy is below 4 MeV. The SEU cross-section for this whole three-layered die-stacked model is smaller than that for die 1 when proton energy is below 1 MeV, the specific reason will be discussed in the next section. There is also a difference in critical proton energy that causes the upset for different layers of the die. The critical proton energy causing the upset of die 1 is about 0.3 MeV, while those of the die 2 and die 3 are around 0.8 MeV and 1 MeV, respectively. Finally, for the range with proton energy of 1.2 MeV–4 MeV, the SEU cross-section values of the three dies are in the order of die 1 > die 2 > die 3, and gradually becomes identical as the proton energy increases.

4. Discussion

4.1. Planar and 3D die-stacked SRAM

To better understand the intrinsic mechanism of SEU in 3D die-stacked devices, we conduct a comparative analysis of planar devices and 3D die-stacked devices. Figure 5 shows the SEU cross-section induced by proton energy in a range of 0.3 MeV–100 MeV for the single-layered die device and the three-layered 3D die-stacked device. As the energy of the incident protons increases from 0.3 MeV to 100 MeV, there appears a big difference in the performance of the SEU cross-section between the two devices. In a proton energy range between 0.3 MeV and 0.9 MeV, the SEU cross-section of the 3D stacked device is three times lower than the total SEU cross-section of the planar device. When the primary energy of the incident proton is greater than 0.9 MeV, the SEU cross-section of the 3D stacked device first increases to the same level as the planar device, then exceeds that of the planar device. Finally, as the incident proton energy continues to increase and reaches to 4 MeV, it gradually becomes the same as the SEU cross-section of the planar device.

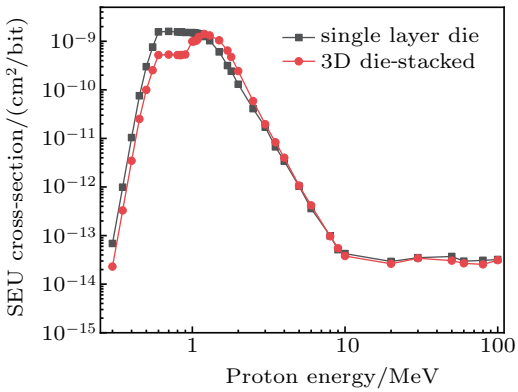

Fig. 5. Proton-induced SEU cross-section *versus* proton energy for 3D die-stacked and planar single-layered SRAM.

Figure 6 shows the curves of proton LET *versus* range in SiO_2 for different incident proton energy values. It is clearly shown that for protons with different initial incident energy values, the range in SiO_2 is also quite different. Of course, after considering the proton range straggling, the final proton range may fluctuate, but it has little effect on the analysis of simulation results. It can be seen from the figure that as the incident proton energy increases, its range in SiO_2 also increases. First, the proton energy can be incident on the die 1 position after the proton energy has been larger than 0.3 MeV, and then the proton range can be incident on the die 2 position when the energy is increased to 0.8 MeV. Finally, when

the proton energy is greater than 0.9 MeV, the proton range is enough to pass through all these three layers of die. The proton's range difference is reflected in the curve of the SEU cross-section. When the primary proton energy is in a range of 0.3 MeV–0.8 MeV, only the top layer die of the 3D device can be incident on the proton and lead to SEU. Comparing with the single-layered die chip, the storage capacity of the 3D die-stacked device is increased by a factor of three. Although the number of upsets is similar, the resulting SEU cross-section is reduced by about three times. When the proton energy increases from 0.8 MeV, the proton range is slowly incident on the second layer and third layer of the three-layered die-stacked device, so the total SEU cross-section also increases rapidly. The Bragg peak of the proton in the device is near the end of its range. When the proton range is sufficient to be incident on the third layer die, the number of upsets caused by protons in the second- and third-layer die is greater than that of the first layer, so the total upset cross-section is larger than that of a single-layered die. Finally, with the further increase of proton energy, the proton can completely penetrate the three layers of dies in the range, and the LET value is similar near each layer of the die. So, the total SEU cross-section is almost the same as that of the planar device.

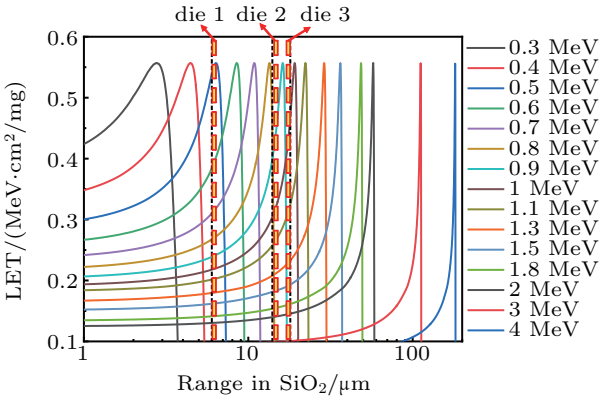

Fig. 6. Curves of LET *versus* range in SiO_2 for different incident proton energy values, (calculated by OMERE[16] software).

In addition, through the above analysis, if we want to reduce the sensitivity of the 3D die-stacked device to SEU caused by LEPs, then we only need to make the spacing between the dies of each layer large enough, regardless of the initial incident proton energy. Then LEP induced SEU through direct ionization mechanism can only affect one single layer of the device.

In this paper, the 3D die-stacked device model has a critical charge of 0.8 fC and the SV has a vertical height of 0.5 μm. Then the critical LET of the device can be calculated to be 0.155 MeV·cm^2/mg. The corresponding proton energy at this LET is 1.44 MeV, and the proton of this energy has a range of 35 μm in SiO_2, which means that only the spacing of each layer of die is greater than 35 μm, the influence of LEP direct ionization can be only in one layer of the device, and it is not possible to affect other layers at the same time. In summary, for the 3D die-stacked device model in this paper, it is necessary only to increase the space of each layer of die to more than 35 μm, which can reduce the SEU sensitivity of the device to LEPs.

4.2. MBU

4.2.1. MBU rate

After analyzing the simulation data, it is found that there are MBUs in addition to the single-bit upset (SBU) for both the single-layered die device and the 3D die-stacked device. For better statistics, we classify the MBU as double-bit upset (DBU) and greater than DBU. Through data analysis, it is found that the highest number of upsets is 4 bits for single-layered die device, whereas, for 3D device, the maximum number of upsets is 6 bits. To quantify the MBU probability, the MBU ratio is calculated from

$$\mathrm{MBU_{ratio}} = \frac{\mathrm{MBU}}{\mathrm{SEU}} \times 100\%,$$

where SEU represents the number of all upset bits, and MBU is the number of incident proton-induced more than one upset. The MBU ratio for the single-layered device and the 3D die-stacked device are depicted in Fig. 7. The proton-induced MBU ratio is a function of incident proton energy in a range from 0.3 MeV to 10 GeV.

As can be seen in Fig. 7, when the incident proton energy is less than 0.7 MeV, the MBU ratio for the single-layered device and the 3D die-stacked device are the same. This phenomenon is attributed to the range limit of incident protons. As shown in Fig. 6, when the incident proton energy is less than 0.7 MeV, its range is insufficient to be incident on the second- or third-layer die of the device. As the incident proton energy increases, when the proton energy is in a range of 0.7 MeV–4 MeV, there is a significant difference in MBU probability between the single-layered die device and the 3D die-stacked device. The single-layered device has almost no MBU, while the MBU probability of 3D device suddenly increases and a peak appears, and the DBU probability increases up to 20.07%. Before the proton incident simulation, we label each SV of the device model, which means that the positional relationship of each error can be easily known when MBU occurs. After analyzing the MBU position information of the 3D device, we find that in this energy segment, the contribution of the MBU mainly comes from the MBU in the incident direction of the particles between the layers, and the MBU of the single layer is very small and can almost be ignored. Also, a large proportion of MBU (> 2) is found in this proton energy range, and the maximum number of upset bits found is four, with a maximum ratio of 4.15% (when the initial proton energy is 1.5 MeV). When the incident proton energy is greater than 4 MeV and continues upward, the trend of the probability of MBU is consistent regardless of whether it is a single-

layered die device or a 3D die-stacked device. As the proton energy increases from 4 MeV, the ratio of MBU increases first for both the single-layered device and the 3D device, then reaches a saturation value, which rarely changes as the proton energy continues to increase. As can be seen from Fig. 7, for the DBU, the saturated MBU (= 2) ratio (16%) appears near the proton energy of 30 MeV, while for the MBU (> 2), the incident proton energy reaching the saturation ratio (7.6%) is higher, around 1000 MeV.

4.2.2. MBU patterns

To analyze the MBU characteristics in more detail, the MBU patterns under different simulation conditions are further studied. The first thing that needs to explain is that the analyzing of MBU patterns is a very complicated job. No matter which energy the proton is incident on the 3D die-stacked device, there are a lot of types of MBU patterns, and when the incident proton fluence increases, some new MBU patterns may appear. Therefore, it is impossible to fully analyze all possible MBU patterns at all incident proton energy values. Several common DBU and triple bit upset (TBU) patterns observed in the simulation for the 3D die-stacked SRAM are shown in Fig. 8. When the incident proton energy is less than 0.9 MeV, since the incident proton range is not enough to be incident on the second layer die of the 3D device, only the DBU appears, and the MBU patterns have only patterns 1 and 4.

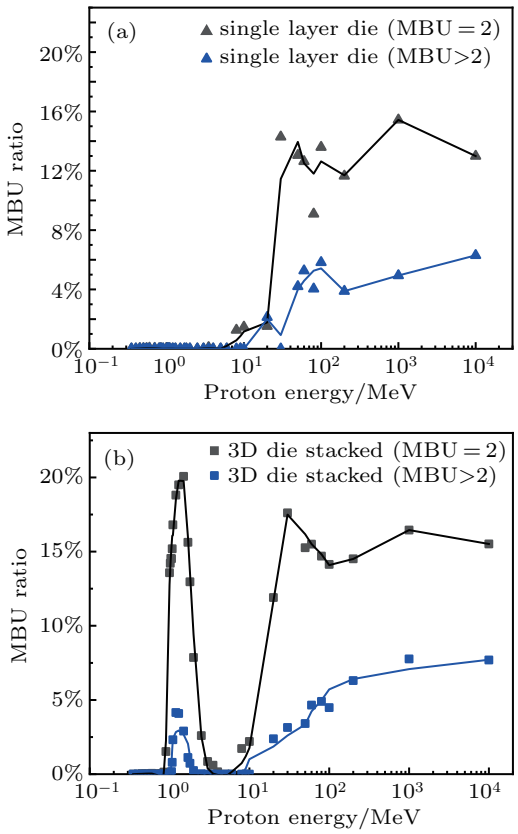

Fig. 7. Curve of ratio of MBU *versus* incident proton energy for (a) the single-layered die device and (b) the three-layered die-stacked device.

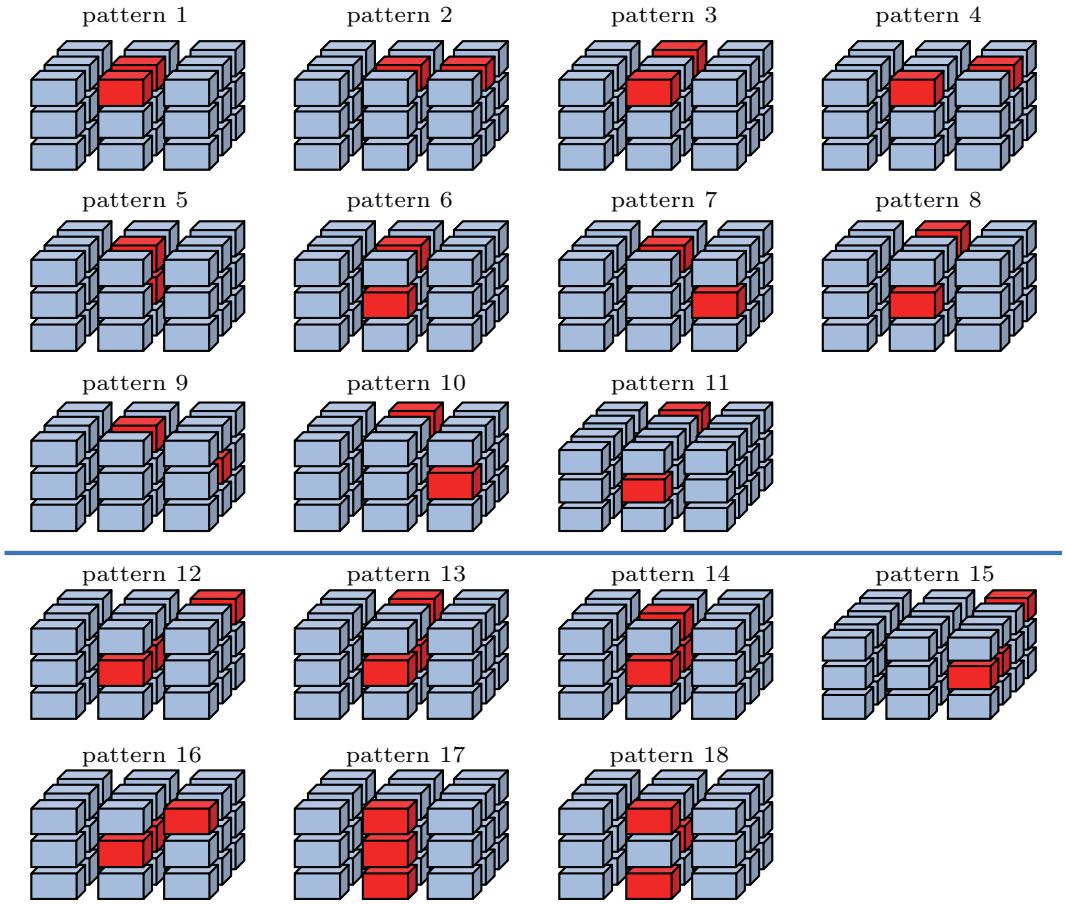

Fig. 8. Example of proton-induced DBU and TBU patterns in 3D die-stacked SRAM, with red box denoting upset cell, and blue box representing normal cell.

Moreover, most of the MBU patterns are pattern 1, and patterns 2–4 appear just occasionally, less than 1% in total. Another interesting result is that when the proton range is sufficient to be incident on multiple layers, the MBU between layers is much higher than that of a single layer. For example, when the incident proton energy is 1.3 MeV, the number of DBUs recorded in the simulation is 123261, and the number of recorded DBUs that occur just in a single layer is just 42.

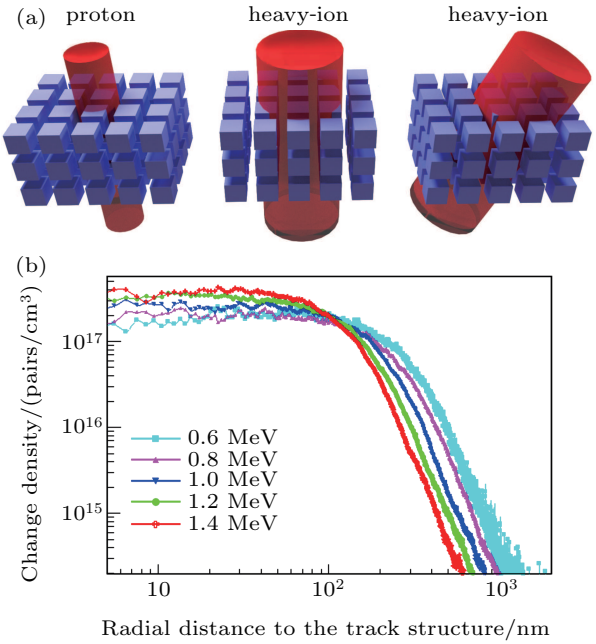

Fig. 9. (a) Schematic diagram of proton and heavy-ion incident into 3D device (not scaled); (b) curves of charge density *versus* radial distance for different initial proton energy values.

In addition, the MBU patterns' formation mainly come from three factors. The first is that when the proton energy is not enough to be incident on the second layer die and is not sufficient to produce a nuclear reaction, it is seen that there are some DBUs of patterns 1 and 4 in the simulation result. As can be seen from Fig. 9, this part of the MBU is caused by the charge sharing induced by LEP direct ionization mechanism. When the proton energy increases, the MBU patterns such as patterns 5 and 6 appear. The source of this partial MBU pattern is mainly the result of the combination of LEP lateral charge sharing and longitudinal proton range influence. The type of MBU patterns caused by the above two reasons is not complicated, but the MBU ratio caused by them is relatively high. Finally, with the further increase of proton energy, the secondary heavy ions generated by the proton nuclear reaction will be the main factor leading to SEU in the 3D device. The difference between secondary heavy ions and incident initial protons mainly lies in the fact that the secondary heavy ion's LET value is higher, while the flux is much lower due to the lower proton nuclear reaction cross-section. It is precise for the above two causes that the SEU of the 3D die-stacked device induced by high-energy protons shows that the total SEU cross section is very low, but the ratio of MBU is high. Moreover, due to the high LET characteristics of the secondary heavy ions and the uncertainty of the direction, the MBU patterns become more diverse.

4.3. On-orbit upset rate analysis

According to the simulation result shown in Fig. 5, the on-orbit upset rate induced by proton for the planar and 3D die-stacked SRAM are predicted by using SPACE RADIATION 7.0.[17] As shown in Table 1, the on-orbit SEU rates under different conditions are calculated for the single-layered device and the 3D die-stacked device. The "ratio" here in the table represents the on-orbit upset rate value of the planar device, divided by the on-orbit upset rate value of the 3D die-stacked device. In order to make the results more credible, MBUs are considered in the calculation process. Obviously, variations in orbit height and Al shielding thickness have a great influence on the on-orbit SEU rate both for the single-layered device and the 3D die-stacked device. Although the orbit height has a great influence on the on-orbit SEU rate, caused by protons, there is no simple linear relationship.

Table 1. On-orbit SEU rate of planar device and 3D die-stacked device. The unit 1 mile = 1.609344 km.

Orbit	Al shield thickness/mile	Proton model	On-orbit upset rate/(errors/device/day)		Ratio
			Planar device	3D die stacked device	
ISS 500 km	100	AP8MIN	2.76×10^{-3}	2.19×10^{-3}	1.260
		AP8MAX	1.01×10^{-3}	8.02×10^{-4}	1.259
	500	AP8MIN	7.44×10^{-4}	5.93×10^{-4}	1.255
		AP8MAX	3.06×10^{-4}	2.44×10^{-4}	1.254
LEO 1200 km	100	AP8MIN	8.82×10^{-2}	7.00×10^{-2}	1.260
		AP8MAX	7.01×10^{-2}	5.56×10^{-2}	1.261
	500	AP8MIN	1.89×10^{-2}	1.51×10^{-2}	1.252
		AP8MAX	1.43×10^{-2}	1.14×10^{-2}	1.254
GEO 35786 km	100	JPL 1991	5.62×10^{-1}	4.45×10^{-1}	1.263
	500	JPL 1991	4.60×10^{-2}	3.65×10^{-2}	1.260

In addition, the proton model used in the calculation has a very large influence on the calculation result. Although the calculation of the proton-induced on-orbit SEU rate of the device is so complicated and has various factors, we can still draw a very useful conclusion after analysis. Regardless of the calculated parameters, the on-orbit SEU rate of the planar device is higher than that of the 3D die-stacked device, and the ratio is maintained at around 1.26.

5. Conclusions

In this work, we build a planar device model and a 3D die-stacked device model, then proton-induced SEU in the planar device and 3D die-stacked device are investigated by toolkit Geant4. The difference in SEU cross-section between these two types of the devices, caused by proton, is discussed. The MBU and on-orbit SEU rate of these two types of devices are also analyzed.

The results show that there is a difference in proton caused SEU cross-section between the two types of devices in an LEP area. The main reason for this difference is that the upper die has a certain shielding effect on the lower die. After analyzing the simulation results, it is found that the MBU ratio of the 3D die-stacked device is higher than that of the single-layered device, and the MBU pattern is more complicated. Finally, through the software SPACE RADIATION 7.0 calculation, it is found that regardless of the orbital parameters, the proton-caused on-orbit error rate of the 3D die-stacked device will be lower than that of the planar device. The result is of significance for aerospace applications of these 3D die-stacked devices.

References

[1] Sadaka M, Radu I and Di C L 2010 2010 *IEEE International Conference on Integrated Circuit Design and Technology*, June 2–4, 2010, Grenoble, France, p. 106

[2] De M K, De M P, Sabuncuoglu T D, Baert K, Beyne E, Mertens R and Van H C 2005 *ESA Round Table Micro/Nano Technol. For Space*, January, 2005, Leuven, Belgium

[3] The 3D-PLUS company homepage: http://www.3d-plus.com

[4] Zhang W and Li T 2008 *Proceedings of the* 41*st Annual IEEE/ACM International Symposium on Microarchitecture*, November 8–12, 2008, Washington, USA, p. 435

[5] Gouker P M, Tyrrell B, Renzi M, Chen C, Wyatt P, Ahlbin J R, Weeden-Wright S, Atkinson N M, Gaspard N J and Bhuva B L 2011 *IEEE Trans. Nucl. Sci.* **58** 2555

[6] Gouker P M, Tyrrell B, D'Onofrio R, Wyatt P, Soares T, Hu W, Chen C, Schwank J R, Shaneyfelt M R and Blackmore E W 2011 *IEEE Trans. Nucl. Sci.* **58** 2845

[7] Sun H, Ren P, Zheng N, Zhang T and Li T 2011 *Microprocess. Microsyst.* **35** 371

[8] Li P, Guo W, Zhao Z and Zhang M 2015 *Computer Engineering and Technology* (Berlin: Springer) p. 164

[9] Han H, Chung J and Yang J S 2018 *IEEE Trans. Comput.* **67** 1193

[10] Song C and Zhang M 2014 *Computer Engineering and Technology* (Berlin: Springer) p. 176

[11] Cao X, Xiao L, Huo M, Wang T, Li A, Qi C and Wang J 2016 arXiv: 1608.01345

[12] Agostinelli S, Allison J, Amako K, Apostolakis J, Araujo H, Arce P, Asai M, Axen D, Banerjee S and Barrand G 2 2003 *Nucl. Instrum. Methods Phys. Res. Sect. A-Accel. Spectrom. Dect. Assoc. Equip.* **506** 250

[13] Heidel D F, Marshall P W, Pellish J A, Rodbell K P, LaBel K A, Schwank J R, Rauch S E, Hakey M C, Berg M D and Castaneda C M 2009 *IEEE Trans. Nucl. Sci.* **56** 3499

[14] Sierawski B D, Pellish J A, Reed R A, Schrimpf R D, Warren K M, Weller R A, Mendenhall M H, Black J D, Tipton A D and Xapsos M A 2009 *IEEE Trans. Nucl. Sci.* **56** 3085

[15] Ye B, Liu J, Wang T S , Liu T Q, Luo J, Wang B, Yin Y N, Ji Q G, Hu P P and Sun Y M 2017 *Chin. Phys. B* **26** 088501

[16] The OMERE software homepage: http://www.trad.fr/en/space/omere-software/

[17] The SPACERAD software homepage: http://www.spacerad.com